

Transverse momentum and pseudorapidity distributions of final-state particles and spatial structure pictures of interacting system in p -Pb collisions at $\sqrt{s_{NN}} = 5.02$ TeV

Fu-Hu Liu^{a,1}, Hua-Rong Wei^a, and Roy A. Lacey^{b,c,2}

^a*Institute of Theoretical Physics, Shanxi University, Taiyuan, Shanxi 030006, China*

^b*Department of Chemistry, Stony Brook University, Stony Brook, NY 11794-3400, USA*

^c*Department of Physics and Astronomy, Stony Brook University, Stony Brook, NY 11794-3800, USA*

Abstract: The transverse momentum and pseudorapidity distributions of final-state particles produced in proton-lead (p -Pb) collisions at center-of-mass energy per nucleon pair $\sqrt{s_{NN}} = 5.02$ TeV are studied in the framework of a multisource thermal model. Experimental results measured by the ALICE and CMS Collaborations are described by the Tsallis transverse momentum distribution and the two-cylinder pseudorapidity distribution. Based on the parameter values extracted from the transverse momentum and pseudorapidity distributions, some other quantities are extracted. Then, the structure pictures of interacting system at the stage of kinetic freeze-out in some spaces are obtained.

Keywords: Transverse momentum distribution, Pseudorapidity distribution, Tsallis statistics, Two-cylinder, p -Pb collisions

PACS Nos.: 25.75.Ag, 24.10.Pa, 25.75.Dw

1 Introduction

High energy collisions are an important research field in modern physics. Since 2000, the Relativistic Heavy Ion Collider (RHIC) has been opening a new era for the collisions, which boosts superlatively the center-of-mass energy per nucleon pair ($\sqrt{s_{NN}}$) to 200 GeV [1–8]. In 2008, the Large Hadron Collider (LHC) ran firstly. Presently, the LHC carries out proton-proton (pp), proton-lead (p -Pb), and lead-lead (Pb-Pb) collisions at different TeV [9–16]. Such high energy collisions give us a chance to study not only the properties of quark-gluon plasma (QGP) and other new physics but also the particle spectra of different distributions and related effects.

A high density and high temperature location is expected to form in high energy nucleus-nucleus collisions which provides a method to create QGP matter and to produce

¹E-mail: fuhuliu@163.com; fuhuliu@sxu.edu.cn

²E-mail: Roy.Lacey@Stonybrook.edu

multiple particles. As an input quantity in nucleus-nucleus collisions, pp collision is very useful to understand the interacting mechanisms of nucleus-nucleus collisions. For the purpose of understanding the nuclear effect and whole collision process, one also needs to study the intervenient proton-nucleus collisions which is the topic of the present work.

Transverse momentum distributions are very important to understand the degrees of transverse excitation and non-equilibrium of interacting system. Different distribution forms are used to describe experimental transverse momentum distributions. Generally, for example, we need a two- or multi-Boltzmann (Fermi-Dirac) distribution or other distributions to describe wide transverse momentum distributions. This renders a two- or multi-temperature emission picture which is in fact to fall into the framework of a multi-source thermal model [17–19]. This also means that the interacting system has temperature changes (fluctuations) from a temperature to another one, which can be described by the Tsallis statistics [20–29].

Pseudorapidity (or rapidity) distributions are very important to understand the longitudinal extension of interacting system and nuclear stopping in heavy ion collisions. A pseudorapidity distribution in whole phase space contains not only the contribution of violent interacting components but also the contribution of leading nucleons. A pseudorapidity distribution in central region contains only the contribution of violent interacting components. A combined analysis on transverse momentum and pseudorapidity distributions can provide abundant information on processes of high energy collisions.

In this paper, in the framework of the multisource thermal model [17–19], we use the Tsallis statistics [20–29] to describe the transverse momentum distributions of final-state particles produced in p -Pb collisions with different centrality intervals at $\sqrt{s_{NN}} = 5.02$ TeV. Meanwhile, the pseudorapidity distribution of charged particles produced in non-single-diffractive (NSD) p -Pb collisions at the same energy is studied by using the same model. The calculated results are compared with the experimental data of the ALICE [30, 31] and CMS Collaborations [32]. Some quantities are then extracted from the comparisons, and structure pictures of interacting system in some spaces are obtained due to the extractions.

2 The model and calculation

In the multisource thermal model [17–19], we assume that many emission sources are formed in high energy collisions. Because different interacting mechanisms exist in the collisions and different event samples are measured in experiments, these sources can be classified into a few groups. The sources in the same group are assumed to stay at a local equilibrium state with a given temperature. We can use different models to describe the local equilibrium state. The final-state distribution is the result of a two- or multi-temperature emission process. For example, we can use a two- or multi-Boltzmann (Fermi-Dirac) distribution to describe the transverse momentum distribution and to obtain two or multiple temperatures. This means that the temperature is in fact to have changes (fluctuations) from a local equilibrium state to another one.

It is not a good choice for us to use the two or multiple distributions to describe the transverse momentum spectra and temperature fluctuations. We hope to use only one

distribution to describe uniformly the spectra, and only one temperature to describe the mean effect of the temperature fluctuations. The good candidate is the Tsallis statistics which is widely used in high energy collisions [20–29]. The Tsallis statistics can be used not only for the whole interacting system but also for the singular source. Although one expects another set of parameters for the latter one, we usually use the same set of parameters for both the whole interacting system and the singular source.

According to the Tsallis statistics, the unit-density function of transverse momentum (p_T) and rapidity (y) for a given type of particles is [20–25]

$$\frac{d^2N}{dydp_T} = C_T p_T \sqrt{p_T^2 + m_0^2} \cosh y \left[1 + \frac{q-1}{T} \sqrt{p_T^2 + m_0^2} \cosh y \right]^{-\frac{q}{q-1}}, \quad (1)$$

where N is the number of particles, $C_T = gV/(2\pi)^2$ is the normalization constant, g is the degeneracy factor, V is the volume, T is the (average) effective temperature over fluctuations in different groups, q is the factor (entropy index) to characterize the degree of non-equilibrium among different groups, and m_0 is the rest mass of the considered particle.

To give solely the transverse momentum distribution, we do an integral for y in Eq. (1). Then, we have the Tsallis transverse momentum distribution to be

$$f_{p_T}(p_T) = \frac{1}{N} \frac{dN}{dp_T} = C_0 p_T \sqrt{p_T^2 + m_0^2} \int_{y_{\min}}^{y_{\max}} \cosh y \left[1 + \frac{q-1}{T} \sqrt{p_T^2 + m_0^2} \cosh y \right]^{-\frac{1}{q-1}} dy \quad (2)$$

which uses the approximation expression $1/(q-1)$ [21–26] instead of $q/(q-1)$ in the power index because q is very close to 1, where C_0 denotes the normalization constant which is proportional to the volume, y_{\max} denotes the maximum rapidity, and y_{\min} denotes the minimum rapidity.

On the pseudorapidity (or rapidity) distribution, in the laboratory or center-of-mass reference frame, these multiple sources are assumed to distribute at different rapidities y_x in the rapidity space. Because of different origins, these sources are expected to form a target cylinder in (left) rapidity interval $[y_{T\min}, y_{T\max}]$ and a projectile cylinder in (right) rapidity interval $[y_{P\min}, y_{P\max}]$. Meanwhile, a leading target nucleon source and a leading projectile nucleon source are expected to form at $y_x = y_T$ and $y_x = y_P$ respectively. In symmetric collisions such as pp or Pb-Pb collisions, we have $y_{T\min} = -y_{P\max}$, $y_{T\max} = -y_{P\min}$, and $y_T = -y_P$. In asymmetric collisions such as p -Pb collisions, we do not have these equations.

To describe a pseudorapidity distribution in whole phase space, we need to consider the contributions of the two cylinders and the two leading nucleon sources. For a pseudorapidity distribution in central region, we need only the contribution of the two-cylinder. That is to say, we can use the two-cylinder pseudorapidity distribution to describe the spectrum in the central region. What we do in the model is only to consider the each contribution of target and projectile nuclei to the central fireball. It does not mean that the central fireball can be completely divided into two separate fireballs. In our analysis, we can obtain T and q for a given type of particles by comparing Eq. (2) with experimental transverse momentum distribution. The obtained values of T and q can be used in the analysis of pseudorapidity distribution.

Based on Eq. (2), we can use the Monte Carlo method to obtain a series of p_T . For the assumption of isotropic emission in the source rest frame, the distributions of space angle θ' and azimuthal angle ϕ' can be given by $f_{\theta'}(\theta') = (1/2) \sin \theta'$ and $f_{\phi'}(\phi') = 1/(2\pi)$ respectively. Correspondingly, we can obtain a series of θ' and ϕ' by the Monte Carlo method. Then, we have the x -component of momentum $p'_x = p_T \cos \phi'$, the y -component of momentum $p'_y = p_T \sin \phi'$, the longitudinal momentum $p'_z = p_T / \tan \theta'$, the momentum $p' = p_T / \sin \theta'$ or $p' = \sqrt{p_T^2 + p_z'^2}$, the energy $E' = \sqrt{p'^2 + m_0^2}$, the rapidity $y' \equiv (1/2) \ln[(E' + p'_z)/(E' - p'_z)]$, and so forth.

In the laboratory or center-of-mass reference frame, we have the rapidity $y = y_x + y'$, the energy $E = \sqrt{p_T^2 + m_0^2} \cosh y$, the momentum $p = \sqrt{E^2 - m_0^2}$, the longitudinal momentum $p_z = \sqrt{p_T^2 + m_0^2} \sinh y$, the x -component of momentum $p_x = p'_x$, the y -component of momentum $p_y = p'_y$, the emission angle $\theta = \arctan(p_T/p_z)$, the pseudo-rapidity $\eta \equiv -\ln \tan(\theta/2)$, the transverse rapidity $y_T \equiv (1/2) \ln[(E + p_T)/(E - p_T)]$, the rapidity in ox axis direction $y_1 \equiv (1/2) \ln[(E + p_x)/(E - p_x)]$, the rapidity in oy axis direction $y_2 \equiv (1/2) \ln[(E + p_y)/(E - p_y)]$, the velocity $\beta = p/E = \sqrt{p_z^2 + p_T^2}/E$, the longitudinal velocity $\beta_z = p_z/E$, the transverse velocity $\beta_T = p_T/E$, the x -component of velocity $\beta_x = p_x/E$, the y -component of velocity $\beta_y = p_y/E$, and so forth. Particularly, let t_0 denote the time interval from initial collision to the stage of kinetic freeze-out, we have the space coordinates of the considered particle at the stage of kinetic freeze-out to be $x = t_0 \beta_T \cos \phi'$, $y = t_0 \beta_T \sin \phi'$, $r_T = t_0 \beta_T$, and $z = t_0 \beta_z$.

We would like to point out that Eqs. (1) and (2) do not contain the contribution of flow effect. For a local equilibrium state, the final state distribution is contributed by the sum of thermal motion and flow effect. In the case of neglecting the flow effect, we may obtain a relative larger (effective) temperature. In the case of considering the flow effect, we have experientially the relations between quantities (p'_x , p'_y , p'_z , and E') of the thermal motion and quantities (p_x , p_y , and p_z) of the thermal motion plus flow effect to be $p_x = (p'_x + \beta_x^{\text{flow}} E') / \sqrt{1 - (\beta_x^{\text{flow}})^2}$, $p_y = (p'_y + \beta_y^{\text{flow}} E') / \sqrt{1 - (\beta_y^{\text{flow}})^2}$, and $p_z = (p'_z + \beta_z^{\text{flow}} E') / \sqrt{1 - (\beta_z^{\text{flow}})^2}$, while β_x^{flow} , β_y^{flow} , and β_z^{flow} denote the x -, y -, and z -components of flow velocity β^{flow} , respectively.

Generally, we can describe the thermal motion by the Tsallis distribution and compare it with experimental transverse momentum distribution to determine β_x^{flow} and β_y^{flow} . Then, p_x and p_y can be obtained in the case of considering the flow effect. The azimuth $\phi = \arctan(p_y/p_x)$, the directed flow $v_1 = \cos \phi$, the elliptic flow $v_2 = \cos(2\phi)$, and the higher flow $v_n = \cos(n\phi)$ can be naturally obtained. In the calculation, the directed transverse motion of the emission source is considered in β_x^{flow} and β_y^{flow} . The directed longitudinal motion of the emission source can be considered in β_z^{flow} or y .

3 Comparisons, discussions, and extractions

Fig. 1 presents the transverse momentum distributions of (a) π^+ , K^+ , and p , as well as (b) π^- , K^- , and \bar{p} produced in p -Pb collisions at $\sqrt{s_{NN}} = 5.02$ TeV, where N_{EV} on the axis denotes the number of events. The symbols represent the experimental data of the CMS Collaboration measured in the rapidity range $|y| < 1$ [32]. The curves are our results

calculated by using the Tsallis transverse momentum distribution [Eq. (2)]. The values of free parameters (T and q), normalization constant (C_0), and χ^2 per degree of freedom (χ^2/dof) are given in Table 1. One can see that the Tsallis distribution describes the experimental data of the considered particles in p -Pb collisions at $\sqrt{s_{NN}} = 5.02$ TeV. The temperature parameter T increases and the non-equilibrium degree parameter q decreases with increase of the particle mass, which maybe reflect non-simultaneous productions of different types of particles. The normalization constant decreases with increase of the particle mass, which will be seen to conflict with the results discussed in Fig. 2.

Fig. 2 shows the transverse momentum distributions of (a) π^\pm , (b) K^\pm , (c) $p + \bar{p}$, and (d) $\Lambda + \bar{\Lambda}$ produced in p -Pb collisions at $\sqrt{s_{NN}} = 5.02$ TeV. The symbols represent the experimental data of the ALICE Collaboration measured in $0 < y < 0.5$ and different centrality (C) intervals [30]. The curves are our results calculated by using the Tsallis transverse momentum distribution [Eq. (2)]. For the purpose of clearness, the results for different C intervals are scaled by different amounts shown in the panels. The values of free parameters, normalization constant, and χ^2/dof are given in Table 1. Once more, the Tsallis distribution describes the experimental data of the considered particles in p -Pb collisions with different centrality intervals. The parameter T decreases and the parameter q increases with increase of the centrality percentage, while T and q increases and decreases with increase of the particle mass respectively. The dependence trend of the normalization constant on the particle mass is different from that in Fig. 1, although the normalization constant increases with increase of the centrality percentage.

In the above descriptions, the experimental data are available in a narrow transverse momentum region [30, 32]. This situation affects the extraction of parameters which may vary in a wide transverse momentum region [33–35]. According to the “soft + hard” model [34, 35], the transverse momentum spectrum is contributed by the sum of soft and hard parts (yields). The soft yields come from the QGP (or usual hadronic matter) and the hard yields come from jets. Generally, the soft yields contribute in a narrow region, and the hard yields contribute in a wide region. In the region considered in the present work, the contribution of soft yields is main, and the contribution of hard yields can be neglected. The parameter values obtained in the present work can be regarded as the result of the soft yields. At the same time, to fix flow velocity, we need azimuthal distribution and more other data. For the purpose of convenience and as the first approximation, we neglect flow velocity in the calculations in Figs. 1 and 2. This treatment is consistent with the general Tsallis statistics [29–29] and our previous work on Pb-Pb collisions at 2.76 TeV [36].

From Table 1 we see that the relationship between C_0 and C is non-linear. Particularly, C_0 has a quick increase in peripheral p -Pb collisions. Qualitatively, nuclear stopping is very small in peripheral p -Pb collisions, then a very large longitudinal extension of the interacting system can be obtained at very large C . This results in a very long interacting region and then a very large C_0 which is proportional to the volume. The situation in central p -Pb collisions (with very small C) is opposite. In peripheral Pb-Pb collisions, the increase of C_0 is small because the interacting region (and then the volume) in central Pb-Pb collisions is also large.

To see clearly the dependences of parameters T and q on C and m_0 in NSD p -Pb collisions at $\sqrt{s_{NN}} = 5.02$ TeV, we present the relations (a) $T - C$ for different particles,

(b) $q - C$ for different particles, (c) $T - m_0$ for different centrality intervals, (d) $q - m_0$ for different centrality intervals, (e) $T - q$ for different particles, and (f) $T - q$ for different centrality intervals in Fig. 3. The symbols represent the parameter values in Table 1 and the lines are our fitted results by linear function

$$Y = aX + b, \quad (3)$$

where Y denotes T or q , and X denotes C , m_0 , or q . The units of T and m_0 are GeV and GeV/ c^2 respectively. The values of coefficients (a and b) and χ^2/dof are given in Table 2. One can see that T decreases and q increases with increase of the centrality percentage. At the same time, T increases and q decreases with increase of the particle mass. There is a negative correlation between T and q not only for different centralities but also for different particles. All the linear relationships presented in Fig. 3 are experimental results.

The dependence trends of T on m_0 , q on m_0 , and T on q in p -Pb collisions in the present work are consistent with those in Pb-Pb collisions in our previous work [36]. Although the dependence trends of T on C and q on C in p -Pb collisions are different from those in Pb-Pb collisions, they are not incompatible. In Pb-Pb collisions, T and q do not show a change with increase of C from 0–5% to 30–40%, and T decreases and q increases with increase of C from 40–50% to 80–90% [36]. The former case can be explained by the large enough interacting region comparing with p -Pb collisions and peripheral Pb-Pb collisions. The later one and p -Pb collisions have no large enough interacting region. Large interacting region results in high T and low q due to more energy deposits and more scattering processes respectively.

Except for the possible non-simultaneous production, we have another explanation on the dependence of T on m_0 . All the temperatures obtained in the present work and our previous work [36] are effective temperatures. If we consider the flow effect, it is expected to obtain a uniform “true” temperature of the source for different particle emissions. This “true” temperature should be less than the weighted average of effective temperatures for different particles due to subtracting the flow effect. Because pions are absolutely the most product in the collisions, the weighted average of effective temperatures is nearly the same as that for pion production. Obviously, in most cases, this “true” temperature is less than the expected critical temperature (130–165 MeV) of the QGP formation [37]. In central p -Pb collisions, the “true” temperature is the closest to the lower limit of the expected critical temperature.

Comparing with the index $q/(q-1)$, the index $1/(q-1)$ gives a smaller q . Combining with our previous work [36], in the case of using the same index, we learn that q in Pb-Pb collisions is less than that in p -Pb collisions. If $q = 1$ corresponds to the equilibrium state, the interacting systems in both p -Pb and Pb-Pb collisions are close to the equilibrium state, and the interacting system in Pb-Pb collisions is closer to the equilibrium state. At the same time, the interacting systems in central collisions are closer to the equilibrium state, and the interacting system consisted of heavier particles is closer to the equilibrium state, too. These results can be explained by the larger interacting region (volume) in central collisions and shorter mean free path of heavier particles.

From Fig. 3 and Table 2, we can see the slopes and intercept points in different linear correlations. The absolute slopes $|a|$'s in $T - C$, $q - C$, $T - m_0$, and $q - m_0$ correlations are less than those in $T - q$ correlations, which renders slow changes in the former cases.

The intercept points b 's in $q - C$ and $q - m_0$ correlations are greater than 1 due to the limitation of physics condition. In $T - C$ and $T - m_0$ correlations, b 's indicate the maximum (122–311 MeV) and minimum (66–91 MeV) temperatures respectively. In $q - C$ and $q - m_0$ correlations, b 's indicate the minimum (1.06–1.13) and maximum (1.14–1.15) non-equilibrium degrees respectively. In $T - q$ correlations, b 's have no physics meaning, because these cases correspond to $q = 0$ which is beyond the limitation of $q \geq 1$. From $T - q$ correlations one can see that q has a value of 1.12–1.21 if the interacting system becomes very cool ($T \rightarrow 0$).

The values of T and q obtained from the above transverse momentum distributions can be used in analysis of pseudorapidity distributions in the same or similar conditions. Fig. 4(a) presents the pseudorapidity distribution of charged particles produced in NSD p -Pb collisions at $\sqrt{s_{NN}} = 5.02$ TeV in the laboratory reference frame, where N_{ch} on the axis denotes the number of charged particles. The circles represents the experimental data of the ALICE Collaboration [31]. The dotted and dashed curves are the contributions of (left target) p -cylinder and (right projectile) Pb-cylinder respectively, and the solid curve is the sum of the two cylinders in which each source is described by the Tsallis statistics. The contributions of leading nucleon sources are neglected. In the calculation, we have distinguished the pseudorapidity and rapidity, and taken the weighted average values of $T = 93 \pm 4$ MeV, $q = 1.142 \pm 0.002$, and $m_0 = 174 \pm 2$ MeV/ c^2 from Fig. 1. Other parameter values obtained by fitting the experimental pseudorapidity distribution are $y_{T \min} = -2.65 \pm 0.08$, $y_{T \max} = 0.01 \pm 0.01$, $y_{P \min} = 0.01 \pm 0.01$, $y_{P \max} = 3.79 \pm 0.10$, and the contribution ratio of target cylinder $K_T = 0.393 \pm 0.002$, with $\chi^2/\text{dof} = 0.046$. One can see that the modelling result is in agreement with the experimental data in the available η range.

Comparing with the pseudorapidity distribution in Fig. 4(a), we give correspondingly the rapidity distribution of charged particles produced in NSD p -Pb collisions at $\sqrt{s_{NN}} = 5.02$ TeV in Fig. 4(b), where the meanings of different curves are the same as those in Fig. 4(a). One can see the difference and similarity between the pseudorapidity and rapidity distributions. By using the same set of parameter values, the distributions of transverse rapidity and rapidities in ox (oy) axis direction for charged particles produced in NSD p -Pb collisions at $\sqrt{s_{NN}} = 5.02$ TeV are given in Figs. 4(c) and 4(d) respectively, where the meanings of different curves are the same as those in Fig. 4(a). One can see that the difference between the contributions of p -cylinder and Pb-cylinder in small y_T (or $|y_{1,2}|$) region is large, and the difference between the two contributions in middle-large y_T (or $|y_{1,2}|$) region is small.

The structure pictures of interacting system (the dispersion plots of final-state particles) in NSD p -Pb collisions at $\sqrt{s_{NN}} = 5.02$ TeV at the stage of kinetic freeze-out in the rapidity spaces (a) $y_2 - y_1$, (b) $y_{1,2} - y_T$, (c) $y_{1,2} - y$, and (d) $y_T - y$ are given in Fig. 5. The circles and squares correspond to the contributions of p -cylinder and Pb-cylinder respectively, where the contributions of leading nucleons are not included. The simulated total number of particles is 1000. Correspondingly, the simulated numbers of particles produced in p -cylinder and Pb-cylinder are 393 and 607 respectively, due to different contribution ratios of the two cylinders. One can see that the densities in small $|y_{1,2}|$ and y_T regions are larger than those in large $|y_{1,2}|$ and y_T regions. There are some zero density regions in the rapidity spaces due to the limitations of kinetics.

The structure pictures of interacting system in NSD p -Pb collisions at $\sqrt{s_{NN}} = 5.02$ TeV at the stage of kinetic freeze-out in the momentum spaces (a) $p_y - p_x$, (b) $p_{x,y} - p_T$, (c) $p_{x,y} - p_z$, and (d) $p_T - p_z$ are presented in Fig. 6. The meanings of the symbols are the same as those in Fig. 5. One can see that the densities in small $|p_{x,y,z}|$ and p_T regions are larger than those in large $|p_{x,y,z}|$ and p_T regions.

The structure pictures of interacting system in NSD p -Pb collisions at $\sqrt{s_{NN}} = 5.02$ TeV at the stage of kinetic freeze-out in the velocity spaces (a) $\beta_y - \beta_x$, (b) $\beta_{x,y} - \beta_T$, (c) $\beta_{x,y} - \beta_z$, and (d) $\beta_T - \beta_z$ are presented in Fig. 7. Meanwhile, the figure is also the structure pictures of interacting system in the same collisions at the stage of kinetic freeze-out in the coordinate space over t_0 : (a) $y/t_0 - x/t_0$, (b) $x/t_0(y/t_0) - r_T/t_0$, (c) $x/t_0(y/t_0) - z/t_0$, and (d) $r_T/t_0 - z/t_0$. The units of quantities in the axes are c , where $c = 1$ in the natural units. The meanings of the symbols are the same as those in Fig. 5. One can see that the densities in small $|\beta_{x,y}|$ and β_T regions and large $|\beta_z|$ region are larger than those in large $|\beta_{x,y}|$ and β_T regions and small $|\beta_z|$ region. Because all the maximum velocities in different directions are close to c , the structure picture of the interacting system in the coordinate space is in fact a sphere which has high densities in near surface regions towards the two beam directions.

4 Conclusions

From the above discussions, we obtain following conclusions.

(a) The transverse momentum distributions of final-state particles produced in p -Pb collisions at LHC energy can be described by the Tsallis distribution which reflects the multiple temperature emission in the multisource thermal model. The calculated results are in agreement with the experimental data of π^\pm , K^\pm , $p + \bar{p}$, and $\Lambda + \bar{\Lambda}$ measured by the ALICE and CMS Collaborations in p -Pb collisions with different centrality intervals at $\sqrt{s_{NN}} = 5.02$ TeV.

(b) The Tsallis transverse momentum distribution uses two free parameters T and q to describe the average temperature and the non-equilibrium degree of the interacting system respectively. The physics condition gives $q \geq 1$. A large q corresponds to a state departing far from equilibrium and $q = 1$ corresponds to an equilibrium state. The present work shows that the values of q are not too large in most cases. This means that the whole interacting system in p -Pb collisions at $\sqrt{s_{NN}} = 5.02$ TeV is close to an equilibrium state. The obtained temperature is less than the lower limit of the expected critical temperature of the QGP formation.

(c) The two parameters (T and q) depend on the impacting centrality and particle mass, and there is a correlation between the two parameters. The present work shows that T decreases and q increases with increase of the centrality percentage, and T increases and q decreases with increase of the particle mass. A negative correlation exists between T and q not only for different centralities but also for different particles in the mentioned collisions.

(d) The pseudorapidity distribution of charged particles produced in NSD p -Pb collisions at $\sqrt{s_{NN}} = 5.02$ TeV can be described by the multisource thermal model in which each source is described by the Tsallis statistics. The contributions of p -cylinder and

Pb-cylinder are given. The parameter values obtained by fitting the transverse momentum and pseudorapidity distributions are used to extract the distributions of rapidities y , transverse rapidities y_T , rapidities y_1 in ox axis direction, and rapidities y_2 in oy axis direction. The contributions of the two cylinders are obviously different in the small y_T or $|y_{1,2}|$ region, and the two contributions are similar in the middle-large y_T or $|y_{1,2}|$ region.

(e) The structure pictures of interacting system in NSD p -Pb collisions at $\sqrt{s_{NN}} = 5.02$ TeV at the stage of kinetic freeze-out in rapidity spaces are extracted. These structure pictures are also the dispersion plots of final-state particles in rapidity spaces. The contributions of p -cylinder and Pb-cylinder are given. The densities in small $|y_{1,2}|$ and y_T regions are larger than those in large $|y_{1,2}|$ and y_T regions. There are some zero density regions in the rapidity spaces due to the limitations of kinetics.

(f) The structure pictures of interacting system in NSD p -Pb collisions at $\sqrt{s_{NN}} = 5.02$ TeV at the stage of kinetic freeze-out in momentum spaces are extracted. These structure pictures are also the dispersion plots of final-state particles in momentum spaces. The contributions of p -cylinder and Pb-cylinder are given. The densities in small $|p_{x,y,z}|$ and p_T regions are larger than those in large $|p_{x,y,z}|$ and p_T regions. There are some zero density regions in the momentum spaces due to the limitations of kinetics.

(g) The structure pictures of interacting system in NSD p -Pb collisions at $\sqrt{s_{NN}} = 5.02$ TeV at the stage of kinetic freeze-out in velocity (coordinate) spaces are extracted. These structure pictures are also the dispersion plots of final-state particles in velocity (coordinate) spaces. The contributions of p -cylinder and Pb-cylinder are given. The densities in small $|\beta_{x,y}|$ and β_T regions and large $|\beta_z|$ region are larger than those in large $|\beta_{x,y}|$ and β_T regions and small $|\beta_z|$ region. The structure picture of the interacting system in the coordinate space is in fact a sphere which has high densities in near surface regions towards the two beam directions.

Acknowledgment

This work was supported by the National Natural Science Foundation of China under Grant No. 10975095, the Open Research Subject of the Chinese Academy of Sciences Large-Scale Scientific Facility under Grant No. 2060205, the Shanxi Provincial Natural Science Foundation under Grant No. 2013021006, the Shanxi Scholarship Council of China under Grant No. 2012-012, and the US DOE under contract DE-FG02-87ER40331.A008.

References

- [1] PHOBOS Collaboration (B.B. Back *et al.*), Phys. Rev. Lett. **87**, 102303 (2001).
- [2] BRAHMS Collaboration (I.G. Bearden *et al.*), Phys. Lett. B **523**, 227 (2001).
- [3] BRAHMS Collaboration (I.G. Bearden *et al.*), Phys. Rev. Lett. **88**, 202301 (2002).
- [4] STAR Collaboration (K.H. Ackermann *et al.*), Phys. Rev. Lett. **86**, 402 (2001).

- [5] PHENIX Collaboration (K. Adcox *et al.*), Nucl. Phys. A **757**, 184 (2005).
- [6] STAR Collaboration (B.I. Abelev *et al.*), Phys. Rev. Lett. **99**, 112301 (2007).
- [7] L.J. Ruan for the STAR Collaboration, J. Phys. G **34**, S199 (2008).
- [8] C.L. da Silva for the PHENIX Collaboration, Indian J. Phys. **85**, 15 (2011).
- [9] ALICE Collaboration (K. Aamodt *et al.*), Eur. Phys. J. C **65**, 111 (2010).
- [10] LHCb Collaboration (R. Aaij *et al.*), Eur. Phys. J. C **71**, 1645 (2011).
- [11] LHCb Collaboration (R. Aaij *et al.*), JHEP **02**, 041 (2013).
- [12] ALICE Collaboration (K. Aamodt *et al.*), Phys. Lett. B **704**, 442 (2011).
- [13] ATLAS Collaboration (G. Aad *et al.*), Nucl. Phys. B **850**, 387 (2011).
- [14] ATLAS Collaboration (G. Aad *et al.*), Phys. Rev D **87**, 052004 (2013).
- [15] CMS Collaboration (V. Khachatryan *et al.*), Phys. Rev. D **83**, 112004 (2011).
- [16] CMS Collaboration (S. Chatrchyan *et al.*), JHEP **02**, 011 (2012).
- [17] F.-H. Liu, Phys. Lett. B **583**, 68 (2004).
- [18] F.-H. Liu, Phys. Rev. C **78**, 014902 (2008).
- [19] F.-H. Liu, Nucl. Phys. A **810**, 159 (2008).
- [20] C. Tsallis, J. Stat. Phys. **52**, 479 (1988).
- [21] C. Tsallis, Braz. J. Phys. **39**, 337 (2009).
- [22] W. M. Alberico, A. Lavagno, Eur. Phys. J. A **40**, 313 (2009).
- [23] G. Wilk, Z. Włodarczyk, Phys. Rev. C **79**, 054903 (2009).
- [24] G. Wilk and Z. Włodarczyk, in *Proceeding of the 6th International Workshop on Relativistic Aspects of Nuclear Physics (RANP2000), São Paulo, Brazil, October 17-20, 2000*, edited by T. Kodama, C.E. Aguiar, H.-T. Elze, F. Grassi, Y. Hama, G. Krein (World Scientific, Singapore, 2001) pp. 78–96, arXiv:hep-ph/0011189v2.
- [25] W. M. Alberico, P. Czerski, A. Lavagno, M. Nardi, V. Somá, arXiv:hep-ph/0510271v2.
- [26] B.-C. Li, Y.-Z. Wang, F.-H. Liu, Phys. Lett. B **275**, 352 (2013).
- [27] T. S. Biró, Eur. Phys. J. A **40**, 255 (2009).
- [28] T. S. Biró, Physica A **392**, 3132 (2013).
- [29] T. S. Biró, G. Purcsel, K. Urmosy, Eur. Phys. J. A **40**, 325 (2009).

- [30] ALICE Collaboration (B. Abelev *et al.*), Phys. Lett. B **728**, 25 (2014).
- [31] ALICE Collaboration (B. Abelev *et al.*), Phys. Rev. Lett. **110**, 032301 (2013).
- [32] CMS Collaboration (S. Chatrchyan *et al.*), arXiv:1307.3442v1, *Eur. Phys. C*, submitted (2013).
- [33] J. Cleymans, D. Worku, Eur. Phys. J. A **48**, 160 (2012).
- [34] K. Urmosy, G. G. Barnaföldi, Sz Harangozó, T. S. Biró, Z. Xu, arXiv:1501.02352v1.
- [35] K. Urmosy, T. S. Biró, G. G. Barnaföldi, Z. Xu, arXiv:1501.05959v1
- [36] F.-H. Liu, Y.-Q. Gao, T. Tian, B.-C. Li, Adv. High Energy Phys. **2014**, 725739 (2014).
- [37] M. Floris, Nucl. Phys. A **931**, 103 (2014).

Table 1. Values of free parameters, normalization constant, and χ^2/dof corresponding to the curves in Figs. 1 and 2. The relative errors for T , q , and C_0 are around 5%, 0.2%, and 5%, respectively.

| Figure | Particle | Centrality | T (GeV) | q | C_0 (fm ³) | χ^2/dof |
|--------|---------------------------|------------|-----------|-------|--------------------------|---------------------|
| 1(a) | π^+ | 0-100% | 0.08 | 1.151 | 204.8 | 0.141 |
| | K^+ | 0-100% | 0.21 | 1.059 | 42.4 | 0.044 |
| | p | 0-100% | 0.25 | 1.067 | 37.1 | 0.059 |
| 1(b) | π^- | 0-100% | 0.08 | 1.151 | 204.8 | 0.097 |
| | K^- | 0-100% | 0.21 | 1.059 | 42.4 | 0.039 |
| | \bar{p} | 0-100% | 0.25 | 1.067 | 37.1 | 0.052 |
| 2(a) | π^\pm | 0-5% | 0.12 | 1.126 | 16.1 | 0.333 |
| | | 5-10% | 0.12 | 1.127 | 14.9 | 0.298 |
| | | 10-20% | 0.11 | 1.134 | 18.7 | 0.227 |
| | | 20-40% | 0.11 | 1.131 | 18.2 | 0.348 |
| | | 40-60% | 0.09 | 1.140 | 34.8 | 0.273 |
| | | 60-80% | 0.08 | 1.144 | 48.0 | 0.314 |
| | | 80-100% | 0.07 | 1.142 | 73.6 | 0.339 |
| 2(b) | K^\pm | 0-5% | 0.18 | 1.110 | 18.3 | 0.068 |
| | | 5-10% | 0.17 | 1.114 | 21.5 | 0.086 |
| | | 10-20% | 0.16 | 1.122 | 23.7 | 0.072 |
| | | 20-40% | 0.16 | 1.115 | 25.6 | 0.099 |
| | | 40-60% | 0.13 | 1.125 | 50.4 | 0.132 |
| | | 60-80% | 0.12 | 1.125 | 64.0 | 0.174 |
| | | 80-100% | 0.10 | 1.123 | 127.3 | 0.173 |
| 2(c) | $p + \bar{p}$ | 0-5% | 0.30 | 1.066 | 11.2 | 0.031 |
| | | 5-10% | 0.29 | 1.065 | 13.0 | 0.037 |
| | | 10-20% | 0.25 | 1.078 | 19.3 | 0.015 |
| | | 20-40% | 0.25 | 1.072 | 21.0 | 0.032 |
| | | 40-60% | 0.20 | 1.082 | 49.7 | 0.111 |
| | | 60-80% | 0.15 | 1.092 | 156.8 | 0.059 |
| | | 80-100% | 0.11 | 1.096 | 678.4 | 0.139 |
| 2(d) | $\Lambda + \bar{\Lambda}$ | 0-5% | 0.31 | 1.062 | 17.6 | 0.134 |
| | | 5-10% | 0.30 | 1.065 | 19.4 | 0.142 |
| | | 10-20% | 0.28 | 1.069 | 22.8 | 0.072 |
| | | 20-40% | 0.24 | 1.078 | 40.3 | 0.075 |
| | | 40-60% | 0.20 | 1.086 | 79.8 | 0.069 |
| | | 60-80% | 0.16 | 1.094 | 211.2 | 0.123 |
| | | 80-100% | 0.13 | 1.096 | 592.6 | 0.354 |

Table 2. Values of coefficients and χ^2/dof corresponding to the lines in Fig. 3. The units of T and m_0 are GeV and GeV/ c^2 respectively.

| Figure | Correlation | Type | a | b | χ^2/dof |
|--------|-------------|---------------------------|--------------------|-------------------|---------------------|
| 3(a) | $T - C$ | π^\pm | -0.059 ± 0.004 | 0.122 ± 0.002 | 0.020 |
| | | K^\pm | -0.087 ± 0.006 | 0.179 ± 0.003 | 0.024 |
| | | $p + \bar{p}$ | -0.212 ± 0.013 | 0.302 ± 0.007 | 0.039 |
| | | $\Lambda + \bar{\Lambda}$ | -0.210 ± 0.008 | 0.311 ± 0.004 | 0.029 |
| 3(b) | $q - C$ | π^\pm | 0.020 ± 0.004 | 1.127 ± 0.002 | 0.004 |
| | | K^\pm | 0.014 ± 0.005 | 1.114 ± 0.003 | 0.008 |
| | | $p + \bar{p}$ | 0.035 ± 0.005 | 1.066 ± 0.002 | 0.007 |
| | | $\Lambda + \bar{\Lambda}$ | 0.041 ± 0.003 | 1.063 ± 0.002 | 0.003 |
| 3(c) | $T - m_0$ | 0-5% | 0.208 ± 0.016 | 0.088 ± 0.012 | 0.084 |
| | | 5-10% | 0.199 ± 0.017 | 0.086 ± 0.013 | 0.139 |
| | | 10-20% | 0.178 ± 0.007 | 0.081 ± 0.005 | 0.047 |
| | | 20-40% | 0.147 ± 0.018 | 0.091 ± 0.014 | 0.121 |
| | | 40-60% | 0.122 ± 0.011 | 0.073 ± 0.009 | 0.068 |
| | | 60-80% | 0.081 ± 0.006 | 0.073 ± 0.005 | 0.070 |
| | | 80-100% | 0.054 ± 0.008 | 0.066 ± 0.254 | 0.006 |
| 3(d) | $q - m_0$ | 0-5% | -0.071 ± 0.007 | 1.139 ± 0.005 | 0.019 |
| | | 5-10% | -0.071 ± 0.009 | 1.141 ± 0.007 | 0.038 |
| | | 10-20% | -0.071 ± 0.007 | 1.149 ± 0.006 | 0.022 |
| | | 20-40% | -0.062 ± 0.009 | 1.141 ± 0.007 | 0.038 |
| | | 40-60% | -0.063 ± 0.009 | 1.150 ± 0.007 | 0.033 |
| | | 60-80% | -0.056 ± 0.006 | 1.151 ± 0.254 | 0.005 |
| | | 80-100% | -0.050 ± 0.004 | 1.148 ± 0.003 | 0.009 |
| 3(e) | $T - q$ | π^\pm | -2.625 ± 0.378 | 3.078 ± 0.429 | 0.130 |
| | | K^\pm | -4.013 ± 1.236 | 4.637 ± 1.384 | 0.424 |
| | | $p + \bar{p}$ | -5.780 ± 0.478 | 6.457 ± 0.516 | 0.101 |
| | | $\Lambda + \bar{\Lambda}$ | -5.056 ± 0.235 | 5.684 ± 0.254 | 0.052 |
| 3(f) | $T - q$ | 0-5% | -2.907 ± 0.095 | 3.399 ± 0.104 | 0.042 |
| | | 5-10% | -2.734 ± 0.119 | 3.207 ± 0.130 | 0.056 |
| | | 10-20% | -2.439 ± 0.154 | 2.885 ± 0.170 | 0.125 |
| | | 20-40% | -2.330 ± 0.104 | 2.751 ± 0.114 | 0.046 |
| | | 40-60% | -1.887 ± 0.107 | 2.246 ± 0.119 | 0.065 |
| | | 60-80% | -1.392 ± 0.165 | 1.678 ± 0.184 | 0.128 |
| | 80-100% | -1.033 ± 0.222 | 1.253 ± 0.247 | 0.218 | |

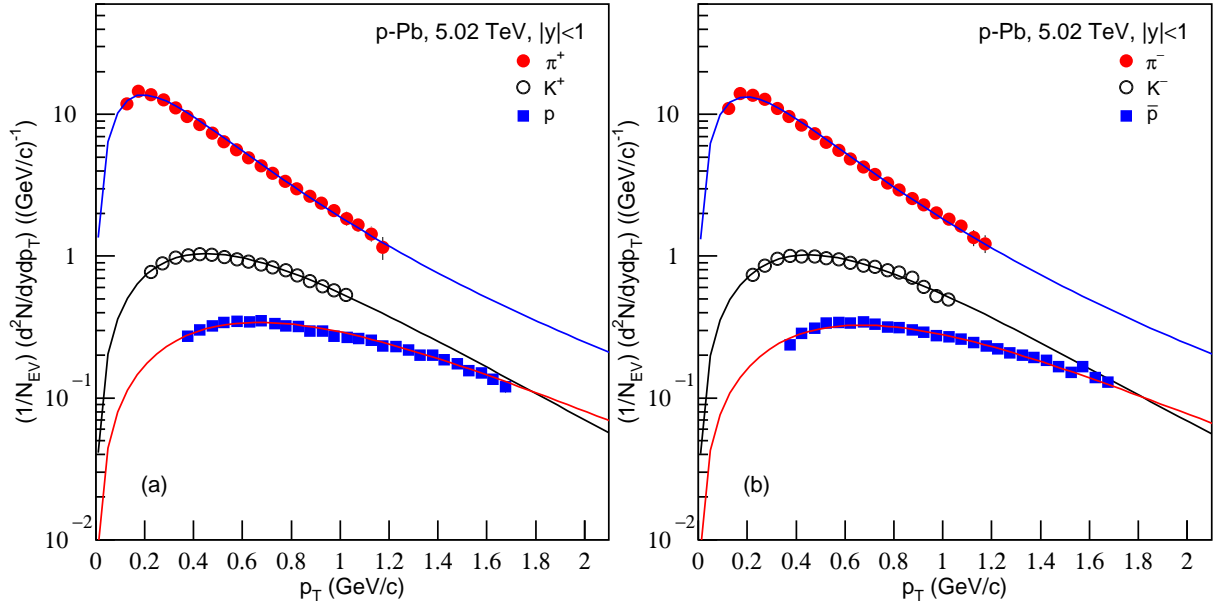


Fig. 1. Transverse momentum distributions of (a) π^+ , K^+ , and p , as well as (b) π^- , K^- , and \bar{p} produced in p -Pb collisions at $\sqrt{s_{NN}} = 5.02$ TeV. The symbols represent the experimental data of the CMS Collaboration [32] and the curves are our results calculated by using the Tsallis transverse momentum distribution.

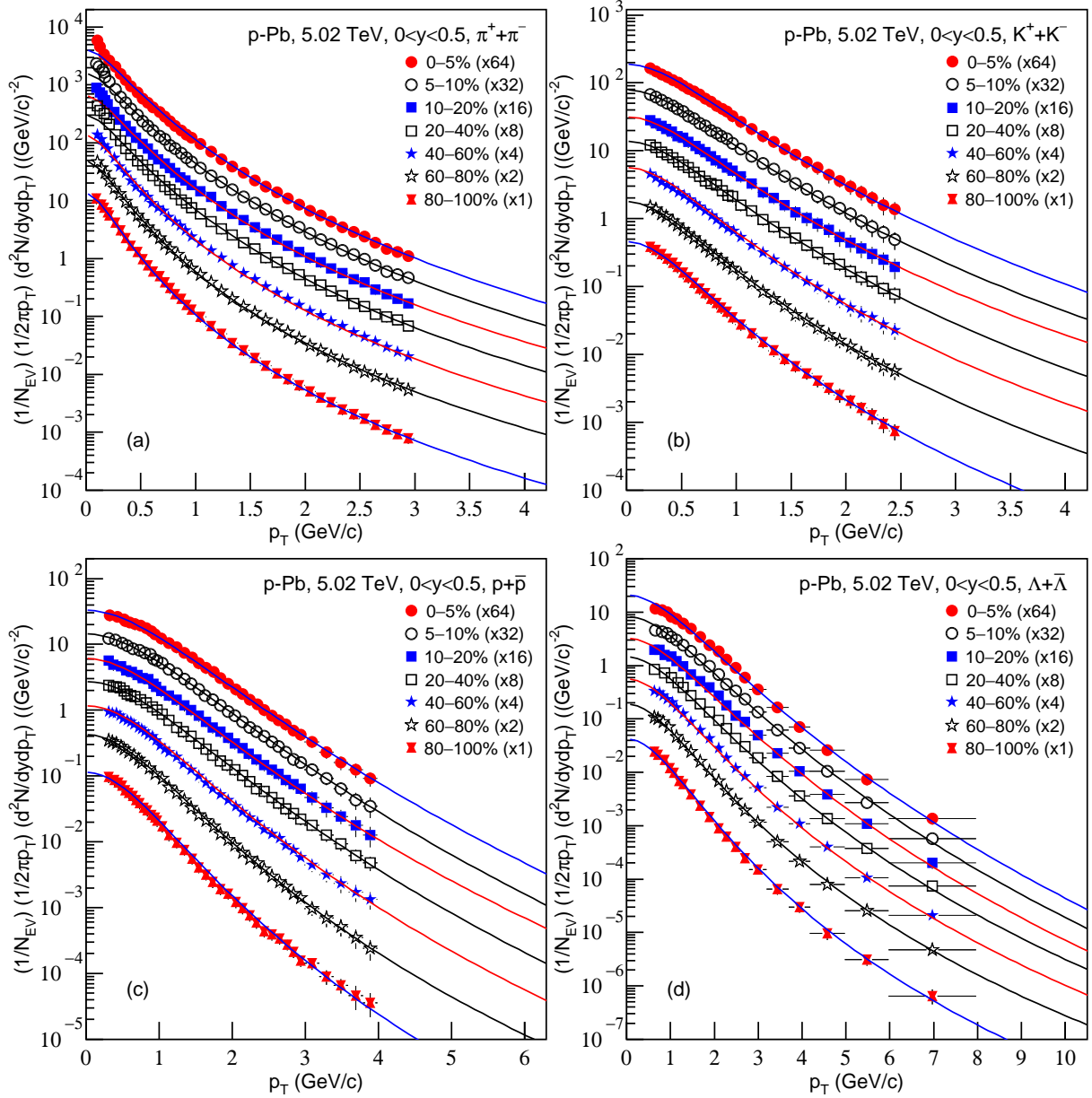


Fig. 2. Transverse momentum distributions of (a) π^\pm , (b) K^\pm , (c) $p + \bar{p}$, and (d) $\Lambda + \bar{\Lambda}$ produced in p -Pb collisions with different centrality intervals at $\sqrt{s_{NN}} = 5.02$ TeV. The symbols represent the experimental data of the ALICE Collaboration [30] and the curves are our results calculated by using the Tsallis distribution.

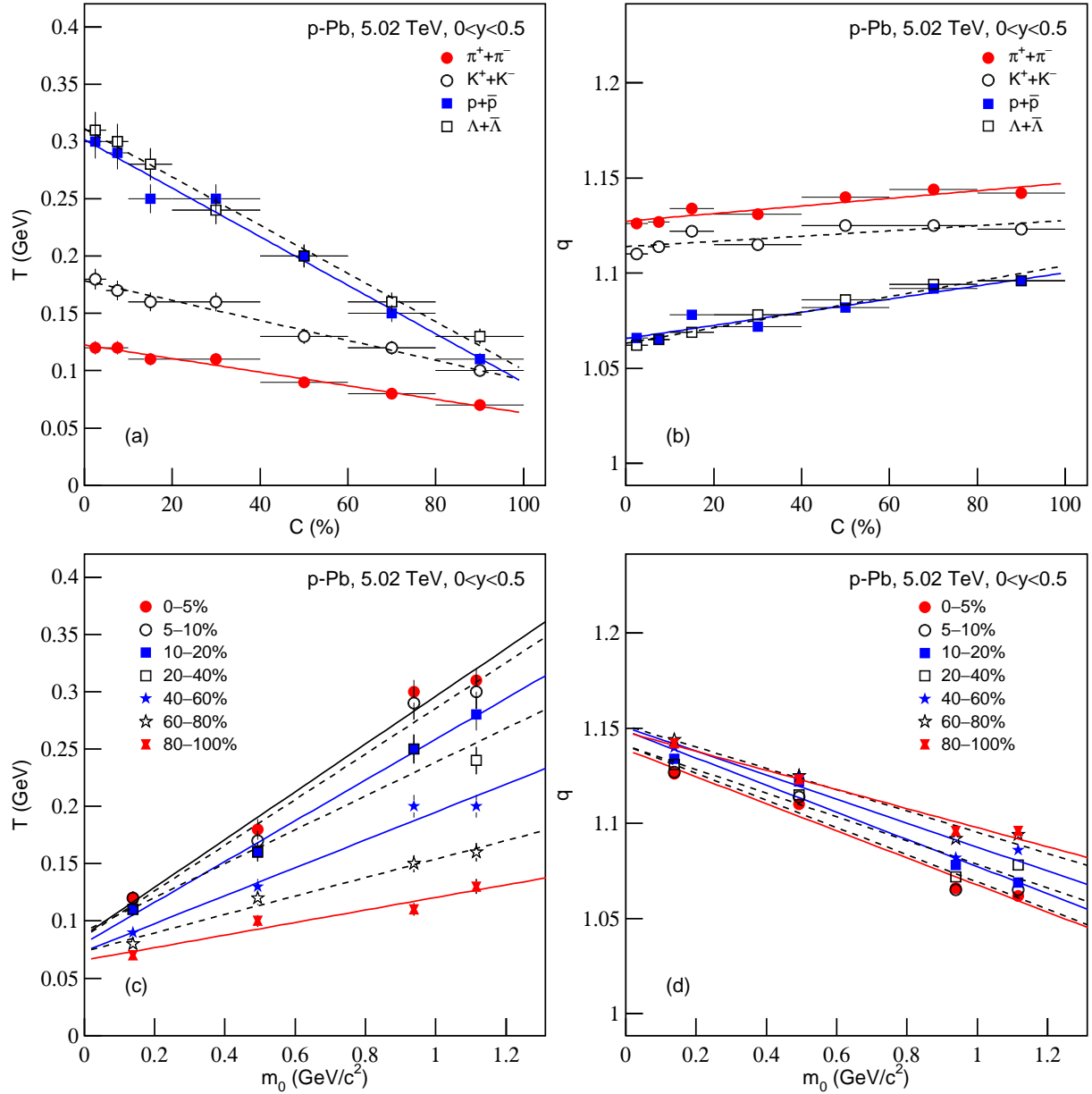


Fig. 3. The relations (a) $T - C$ for different particles, (b) $q - C$ for different particles, (c) $T - m_0$ for different centrality intervals, (d) $q - m_0$ for different centrality intervals, (e) $T - q$ for different particles, and (f) $T - q$ for different centrality intervals, in p -Pb collisions at $\sqrt{s_{NN}} = 5.02$ TeV. The symbols represent the parameter values listed in Table 1, and the lines are our fitting results.

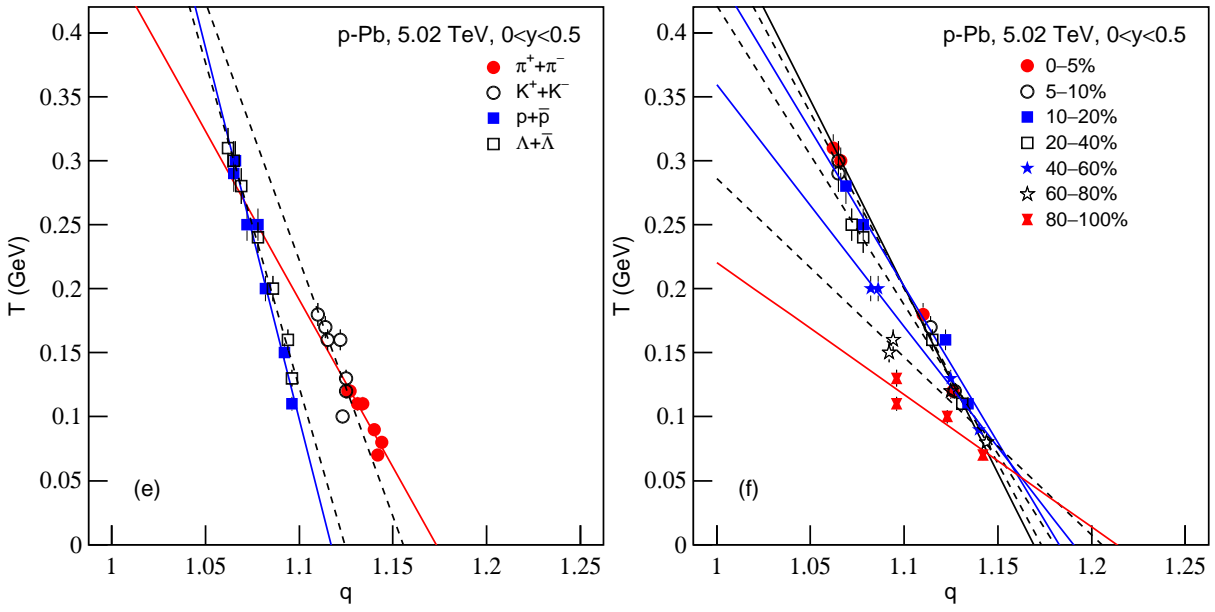


Fig. 3. Continued.

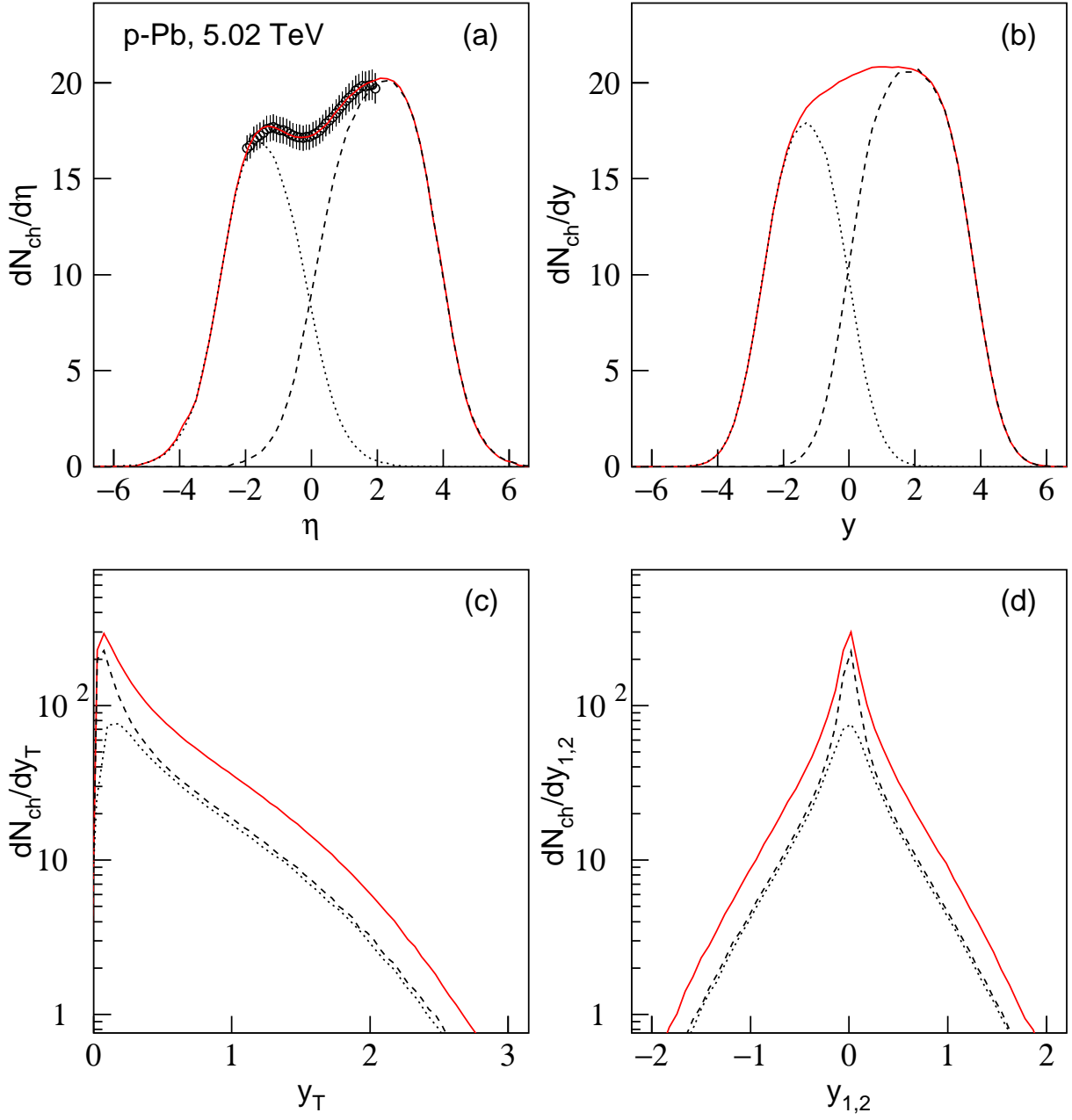


Fig. 4. (a) Pseudorapidity distribution of charged particles produced in NSD p -Pb collisions at $\sqrt{s_{NN}} = 5.02$ TeV. The circles represents the experimental data of the ALICE Collaboration [31] and the curves are our modelling results. The dotted, dashed, and solid curves are the contributions of p -cylinder, Pb-cylinder, and both the cylinders, respectively. (b)-(d) Correspondingly distributions of (b) rapidities, (c) transverse rapidities, and (d) rapidities in ox (oy) axis direction, in the mentioned collisions.

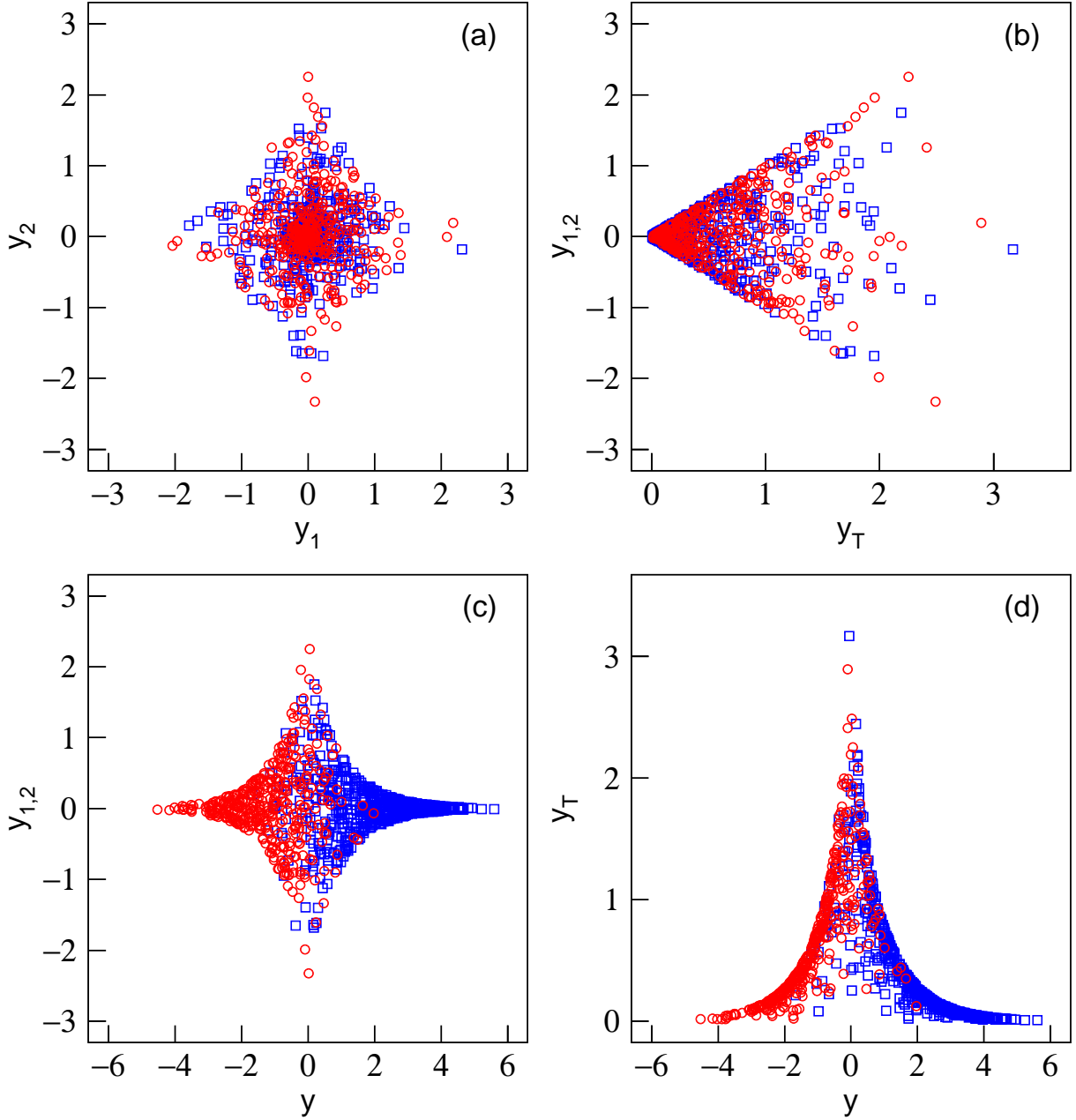


Fig. 5. Structure pictures of interacting system at the stage of kinetic freeze-out in the rapidity spaces (a) $y_2 - y_1$, (b) $y_{1,2} - y_T$, (c) $y_{1,2} - y$, and (d) $y_T - y$, in NSD p -Pb collisions at $\sqrt{s_{NN}} = 5.02$ TeV. The circles and squares represent the contributions of p -cylinder and Pb-cylinder respectively. The contributions of leading nucleons are not included.

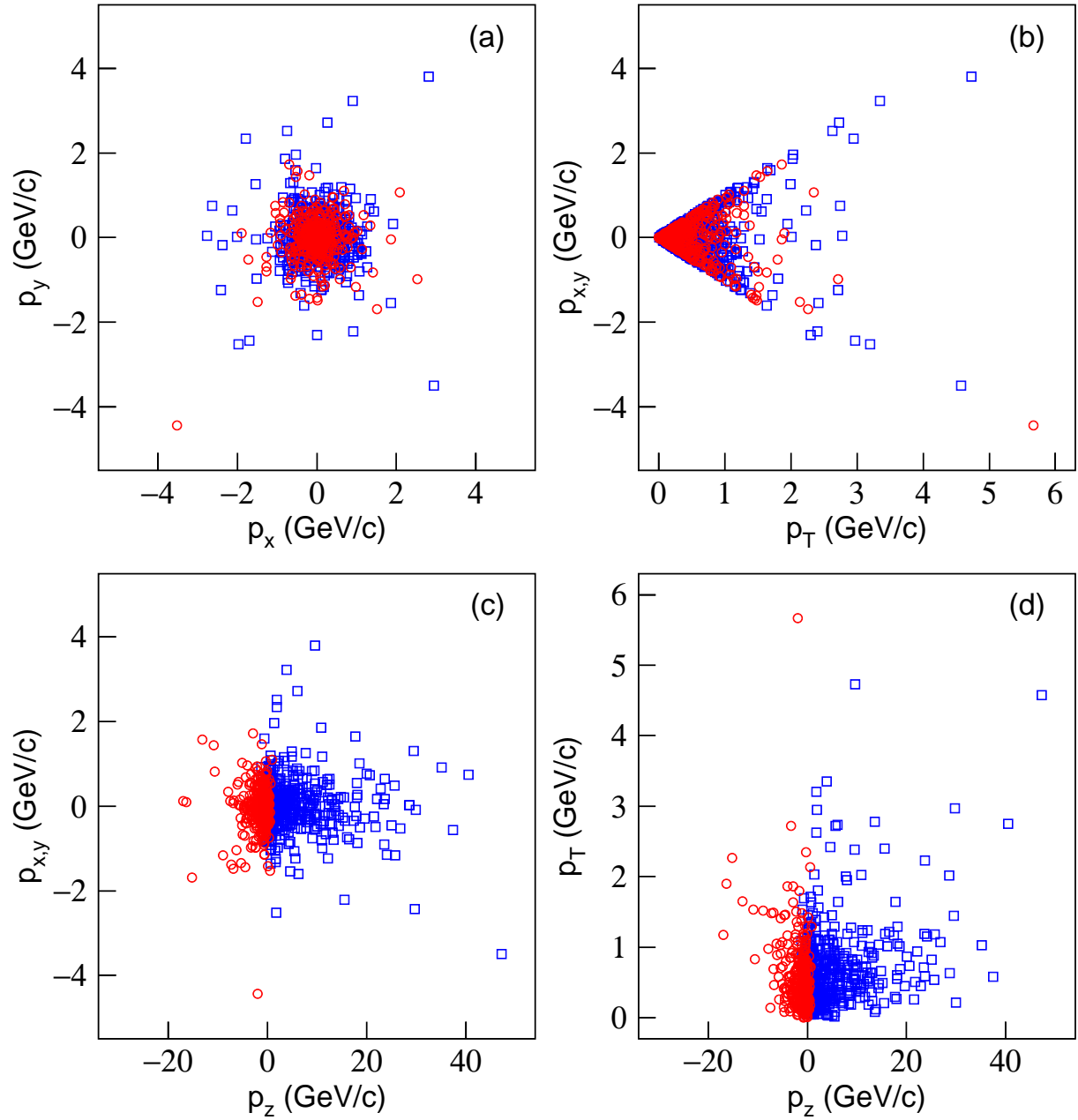


Fig. 6. As for Fig. 5, but showing the structure pictures of interacting system at the stage of kinetic freeze-out in the momentum spaces: (a) $p_y - p_x$, (b) $p_{x,y} - p_T$, (c) $p_{x,y} - p_z$, and (d) $p_T - p_z$.

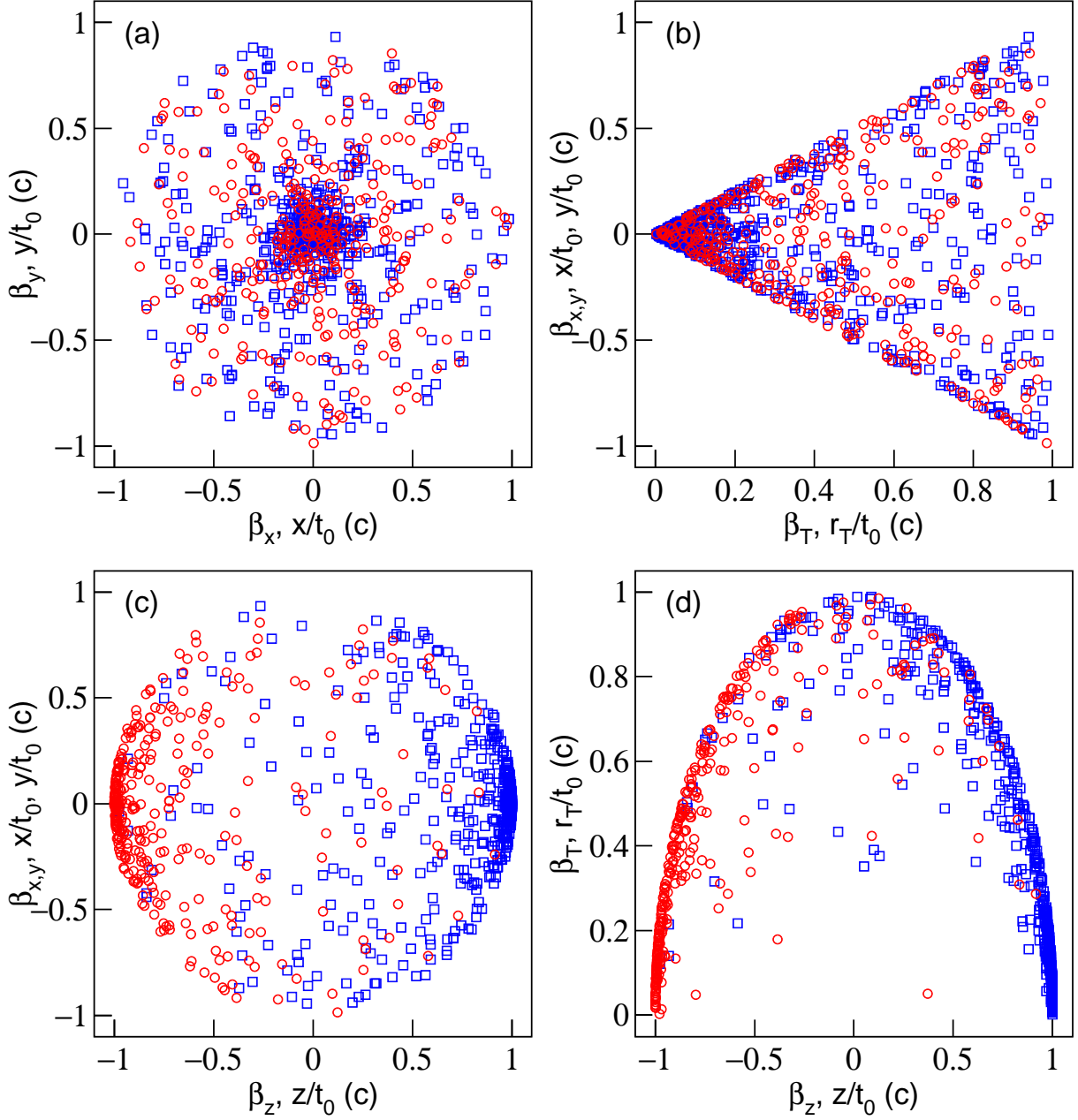


Fig. 7. As for Fig 5, but showing the structure pictures of interacting system at the stage of kinetic freeze-out in the velocity spaces: (a) $\beta_y - \beta_x$, (b) $\beta_{x,y} - \beta_T$, (c) $\beta_{x,y} - \beta_z$, and (d) $\beta_T - \beta_z$; or in the coordinate space over t_0 : (a) $y/t_0 - x/t_0$, (b) $x/t_0(y/t_0) - r_T/t_0$, (c) $x/t_0(y/t_0) - z/t_0$, and (d) $r_T/t_0 - z/t_0$.